Cable-Based Robotic Crane (CBRC): Design and Implementation of Overhead Traveling Cranes Based on Variable Radius Drums

Lorenzo Scalera, Paolo Gallina, Stefano Seriani, and Alessandro Gasparetto

***Abstract*—In this paper, we present a new family of overhead traveling cranes based on variable radius drums (VRDs), called cable-based robotic cranes (CBRCs). A VRD is characterized by the variation of the spool radius along its profile. This kind of device is used, in this context, for the development of a cable-robot, which can support and move a load through a planar working area with just two degrees of freedom. First we present the kinematic analysis and the synthesis of the geometry of a VRD profile. Then, the schema of a bidimensional horizontal moving mechanism, based on the VRD theory, and an experimental prototype of a three-dimensional CBRC are presented. The features of this wire-based overhead crane and an analysis of cables tensions are discussed. Finally, the performance of this mechanism is evaluated, demonstrating a deviation between the end-effector and the nominal planar surface of less than 1% throughout the whole working area.**

***Index Terms*—Cable robot, cable-based robotic crane (CBRC), overhead traveling crane, profile synthesis, variable radius drum (VRD).**

I. Introduction

CABLE robots are a special class of manipulators in which flexible cables, rather than rigid links, are used to actuate the end-effector. The main advantages of this class of robot over conventional ones are that cable-based robots can have a larger workspace, they can easily be made to be reconfigurable and modular [1], they are lighter than their rigid-links counterparts, they can be easily transported, and their end-effector can achieve high accelerations and velocities. For these reasons, during recent years, cable-driven systems have received attention and different kind or cable robots have been investigated. Applications of cable robots span from heavy load and large-scale manipulation [2]–[5], building tasks [6], [7], to rescue operations [8] and upper limbs rehabilitation [9], [10]. Cables have also been employed in surgical robots to reduce surgeon fatigue and facilitate supervised telesurgery [11]–[14]. Cable-suspended robots are also used to manoeuvre aerial camera systems (sky-cams or spider-cams) over large areas, such as a stadium [15], [16]. Several cable-suspended parallel robots have been studied and implemented in the recent years. Examples can be found in [17]–[19].

Disadvantages of a cable-based robotic system include redundancy (as cables can carry load in tension but not in compression) and interference between cables and environment. For these reasons, several research works have been conducted over the years, especially for control purposes [20]–[23], dynamic modeling, and trajectory tracking [24].

Since cables are used in power transmissions, drive systems, and load handling, drums and pulleys have been used in different kind of applications. A drum, or spool, consists of a spindle with flanges, around which a cable is wrapped. The cylindrical surface of an ordinary drum has a constant radius [25]. A typical device, in which an ordinary drum is employed, is a winch [26]. It essentially consists of a movable drum around which a cable is wrapped, so that the rotation of the drum produces a drawing force at the end of the cable. Winches are usually equipped with a ratchet wheel and a pawl to prevent slippage of the load [27].

Examples of research studies in cable-drum systems can be found in [28], where a cable mechanism is used as a linear motion sensor, in [29], where a study on the prediction of slip in a cable-drum system is proposed, and in [25], where the transmission backlash of a precise cable drive system is analyzed and experimentally measured.

While traditionally drums and winches are characterized by a constant radius, in this paper, we propose the use of a variable radius drum (VRD), a mechanical device consisting of a drum with a radius that changes along its profile. As the VRD is rotated by an angle α, a correspondent length of cable is released or wound. This length can be expressed by a nonlinear function $g = g(\alpha)$, which depends on the VRD profile and on the angular position. With respect to constant radius drums with radius r, where the length of the released cable is given by the linear function $g = \alpha\, r$, in a VRD, it is possible to synthesize a specific profile shape in order to obtain the desired relationship $g = g(\alpha)$. Furthermore, in a VRD, a specific profile shape can be defined in order to modify the value of the torque generated by

Manuscript accepted December 31, 2017.

L. Scalera and A. Gasparetto are with the Polythecnic Department of Engineering and Architecture, University of Udine, Udine 33100, Italy (e-mail: scalera.lorenzo@spes.uniud.it; alessandro.gasparetto@uniud.it).

P. Gallina is with the Department of Engineering and Architecture, University of Trieste, Trieste 34127, Italy (e-mail: pgallina@units.it).

S. Seriani is with the DLR Institute for Robotics and Mechatronics, Wessling D-82234, Germany (e-mail: stefano.seriani@dlr.de).

the cable on the VRD itself [30]. The concept of the VRD has been introduced in [31].

This paper presents a new family of overhead traveling cranes based on VRDs. These cable-driven mechanisms are capable of supporting and moving a load on a planar working area, by using just two degrees-of-freedom (DOFs).

Section II briefly summarizes related works that can be found in the literature, Section III gives a general description of a cable-based robotic crane (CBRC), Section IV presents the direct kinematic analysis as well as the synthesis of a VRD, whereas in Section V, a bidimensional horizontal moving mechanism, based on a VRD, is proposed. Section VI reports the inverse kinematic and dynamics of the CBRC, whereas Section VII, an analysis of cable tensions. The experimental prototype of the three-dimensional (3-D) CBRC is presented in Section VIII, whereas in Section IX, the experimental results and the performance of this mechanism are presented. Finally, Section X gives the conclusions of this work.

II. Related Works

Several examples of the VRD can be found in the literature. Endo *et al.* proposed a new weight compensation mechanism with a noncircular pulley and a spring [32]. Kilic *et al.* used a wrapping cams mechanism in the synthesis of nonlinear torsional spring [33], whereas a similar methodology has been used by Schmit and Okada to develop a nonlinear rotational spring [34]. Furthermore, a nonconstant radius pulley for antagonistic springs was proposed by Kim and Deshpande [35]. Shin *et al.* developed a methodology to synthesize variable radius pulleys to improve joint torque capacity in pneumatic artificial muscles, used as actuators for stanford human-friendly robot [36]. An application of the VRD in locomotion is given by Kljuno *et al.*, who developed RoboCat, a quadruped cable-driven robot [37]. From a kinematic point of view, the synthesis of a VRD was approached by Gallina on a particular case of a rocker-belt mechanism [38].

Concerning traditionally overhead cranes, the main research area is, nowadays, the dynamical modeling and control, in order to eliminate swing effects and ensure system stability. Examples can be found in [4] and [39]–[42].

With respect to traditionally overhead cranes, CBRCs do not require rails or linear guides along the whole span of the system since they are essentially composed of a series of pulleys, drums, and cables. For this reason, their frame is lighter and can be easily disassembled. Furthermore, they are modular and their accuracy only depends on the positioning of the pulleys supports in the set-up phase. Cartesian robots are characterized by a high stiffness and are employed in the handling of small workspaces, where they are extremely accurate for high precision pick-and-place tasks. On the contrary, our device is meant for the handling of large amount of materials in very large workspaces, where the weight of the structure can be a problem. One possible application could be the loading and unloading of materials and supplies for general naval applications, where the workspace is large, the infrastructures have to be light and accuracy is much less demanding. Furthermore, the proposed mechanism could also be deployed as a two-dimensional aerial overhear conveyor for industrial or even mining application, where vertical motion is not required. On the other hand, it has to be noticed that in the cases in which a movement of the load in the vertical direction is needed (such as for pick-and-place tasks), a winch could be mounted on the end-effector of the robotic crane.

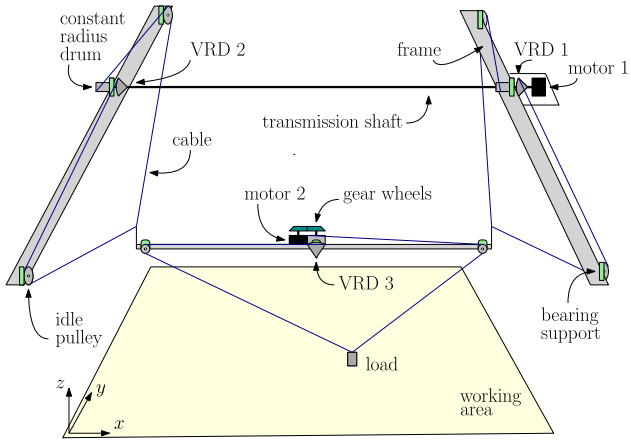

Fig. 1. Graphical representation of a cable-based robotic crane.

To the best of the authors' knowledge, no examples of overhead traveling cranes based on cables and VRDs can be found in the previous literature.

III. CBRC Description

In this section the description of a CBRC is presented. A graphic representation of this 3-D overhead traveling crane based on VRDs can be seen in Fig. 1.

The experimental prototype is composed of three horizontal moving cable mechanisms (HMCMs) identical in size that allow the motion of a load within a planar working area. The two upper mechanisms, identified by VRDs 1 and 2, are positioned at the same vertical height in a parallel position. The end-effector of each of these two upper systems is then connected to one edge of the frame of the third mechanism. Thereby, the lower frame, identified by VRD 3, can be moved horizontally through the y-axis. HMCMs 1 and 2 are connected by means of a transmission shaft, which ensures that they have the same angular position α. The third HMCM is located on the lower frame and enables the motion of the load through the x-axis. In this way, the two DOFs CBRC allows the motion of a load through a rectangular working area.

The CBRC prototype is actuated by two motors: the first is directly connected to the upper transmission shaft and ensures the motion through the y-axis, whereas the second, which ensures the actuation along the x-axis, is located on the shifting frame and transmits the motion to VRD 3 by means of two gear wheels.

IV. Kinematic Analysis and Synthesis

In this section, the kinematic analysis of a VRD for each HMCM is briefly summarized. In Fig. 2, a graphical representation of the VRD is reported. On the left, the VRD is constrained

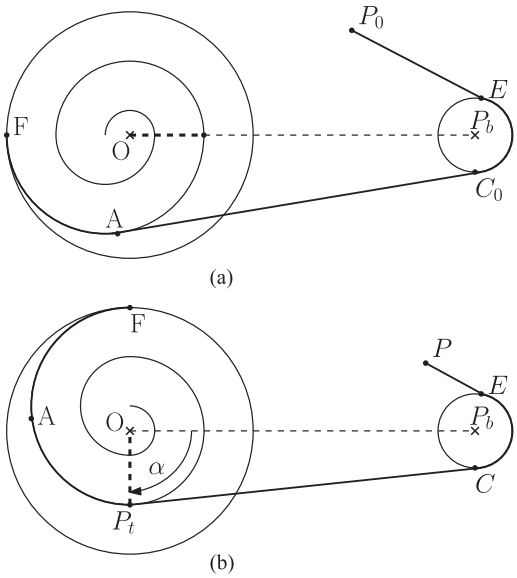

Fig. 2. Kinematic analysis of a variable radius drum.

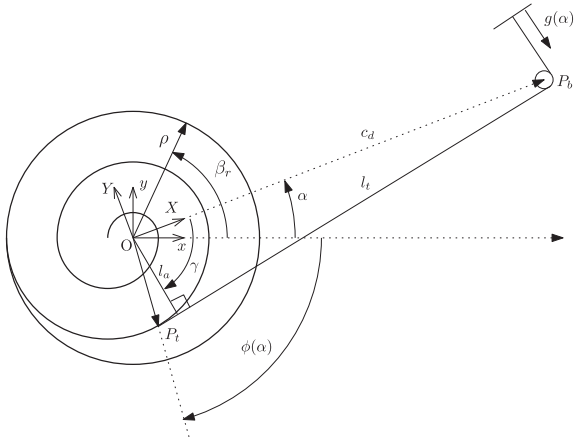

Fig. 3. Variable radius drum parameters in case of point-like idle pulley and neglected cable thickness.

in point $\boldsymbol{O}$ by means of a revolute joint, whereas on the right, an idle pulley is fixed in point $\boldsymbol{P}_b$ with another joint of the same type. The cable is fixed at one end of the VRD in point $\boldsymbol{F}$, it is wound around the drum profile and, initially, it is separated from the VRD in the tangent point $\boldsymbol{P}_t$. We define $\boldsymbol{A}$ as this tangent point fixed at the VRD, at initial conditions, as shown in Fig. 2(a). The cable is then wrapped around the idle pulley and it is tangent to its surface in points E and $\boldsymbol{C}_0$. On the VRD, a marker has been placed in order to easily identify the rotation of the drum with respect to the reference frame, given by angle α. We assume α positive in the clockwise direction. In order to introduce the parameters that characterize the kinematic analysis of the VRD, we consider two different configurations of the drum: the case with $\alpha = 0$ and the one with $\alpha > 0$, reported, respectively, in Fig. 2(a) and (b).

1) Case $\alpha = 0$: In this configuration, we assume that the system is in equilibrium. A proper torque acting on the VRD along the counter-clockwise direction is present as well as a force that pulls the cable and balance the torque action.

When $\alpha = 0$, we define l_0 as the total length of free cable, not wound around the drum, from point $\boldsymbol{P}_0$ to the tangent point $\boldsymbol{A}$. The length of l_0 is given by

$$l_0 = ||\boldsymbol{AC}_0|| + \widehat{\boldsymbol{C}_0\boldsymbol{E}} + ||\boldsymbol{EP}_0||. \tag{1}$$

With the symbol $\widehat{*}$ we indicate arcs as well as curved segments on the VRD.

2) Case $\alpha > 0$: In this configuration, the drum has rotated in the clockwise direction of an angle $\alpha > 0$. A segment of cable length $\widehat{\boldsymbol{AP}_t}$ is wound around the VRD. The length of the segment $\boldsymbol{PE}$ has now changed with respect to the previous configuration: in particular, the length of $\boldsymbol{PE}$ is a function of α and of the shape of the VRD. We obtain

$$||\boldsymbol{P}_t\boldsymbol{C}|| + \widehat{\boldsymbol{CE}} + ||\boldsymbol{EP}|| = l_0 - \widehat{\boldsymbol{AP}}_t. \tag{2}$$

The length of cable wound by the VRD during its rotation is a function of angular position. We define this function $g(\alpha)$

$$g(\alpha) := ||\boldsymbol{EP}_0|| - ||\boldsymbol{EP}||. \tag{3}$$

By replacing (1) and (2) into (3), we obtain

$$g(\alpha) = (||\boldsymbol{P}_t\boldsymbol{C}|| - ||\boldsymbol{AC}_0||) + (\widehat{\boldsymbol{CE}} - \widehat{\boldsymbol{C}_0\boldsymbol{E}}) + \widehat{\boldsymbol{AP}}_t. \tag{4}$$

Three addends contribute in (4): the first is the difference between the length of the cable tangent to the VRD and the idle pulley in case $\alpha = 0$ and $\alpha > 0$, the second is the difference between arcs on the idle pulley when $\alpha = 0$ and $\alpha > 0$, the third is the curved profile of the VRD on which the cable is wound.

A. Direct Kinematic Analysis

The direct kinematic analysis aims to calculate the relationship between the function of wound cable $g(\alpha)$ and the angular position of the VRD α, by knowing the geometry of the VRD profile. In order to do so, we define $\phi = \phi(\alpha)$ as the angle of the tangent point P_t with respect to the horizontal line and considered positive in the clockwise direction (see Fig. 3). We express the profile of the VRD geometry in polar coordinates, as $\rho = \rho(\beta_r)$. We assume the angle β_r positive in the counter-clockwise direction with respect to the frame fixed to the VRD (relative reference frame). Then, the direct kinematic analysis can be developed by solving the integral of the VRD curve:

$$g(\alpha) = (||\boldsymbol{P}_t\boldsymbol{C}|| - ||\boldsymbol{AC}_0||) + (\widehat{\boldsymbol{CE}} - \widehat{\boldsymbol{C}_0\boldsymbol{E}}) + \int_{-\phi(0))}^{\alpha-\phi(\alpha)} \sqrt{\rho^2 + (d\rho/d\beta_r)^2}\, d\beta_r. \tag{5}$$

In (5), both the addends $(||\boldsymbol{P}_t\boldsymbol{C}|| - ||\boldsymbol{AC}_0||)$ and $(\widehat{\boldsymbol{CE}} - \widehat{\boldsymbol{C}_0\boldsymbol{E}})$ are nonlinear functions of the angular position α. Their calculation depends on the function $\rho(\beta_r)$ and it has to be analyzed case by case.

B. Variable Radius Drum Synthesis

In Fig. 3, it can be seen that as the VDR rotates in the clockwise direction, the idle pulley is seen, by an observer on the drum, rotating in the counter-clockwise direction of the same angle. The unit vectors $\boldsymbol{x}$ and $\boldsymbol{y}$ define the reference frame of the VRD, whereas the unit vectors $\boldsymbol{X}$ and $\boldsymbol{Y}$ define the inertial reference frame, with respect to the VRD, fixed to the idle pulley center $\boldsymbol{P}_b$. In this initial approach to the problem, the idle pulley is assumed to be point-like, with a radius equal to zero. In this configuration, we define c_d as the distance between the idle pulley and the center of the VRD, l_t as the distance between tangent point $\boldsymbol{P}_t$ and the idle pulley center, and γ as the angle between the segment $\boldsymbol{OP}_b$ and the minimum distance between the cable and the center $\boldsymbol{O}$ of the VRD. The aim of the synthesis is to calculate the profile of the VRD by knowing the wound cable length function $g(\alpha)$.

In local coordinates, the tangent point $\boldsymbol{P}_t$ can be written as a sum of two vectors: the first from $\boldsymbol{O}$ and $\boldsymbol{P}_b$, $\{c_d \;\; 0\}^T$, the second from $\boldsymbol{P}_b$ and $\boldsymbol{P}_t$, $\{l_t \;\; 0\}^T$:

$$\boldsymbol{P}_t = \boldsymbol{T}(\alpha)\left\{ \begin{array}{c} c_d \\ 0 \end{array} \right\} + \boldsymbol{T}(\alpha)\boldsymbol{T}(-\gamma)\boldsymbol{T}\left(-\frac{\pi}{2}\right)\left\{ \begin{array}{c} l_t \\ 0 \end{array} \right\} \quad (6)$$

where the operator $\boldsymbol{T}(x)$ is the rotation matrix between two reference frames rotated by an angle x.

The whole mathematical derivations to obtain the VRD profile synthesis are reported in Appendix A. Finally, the geometry of the VRD profile, in Cartesian coordinates, is given by the following equation [(31) in Appendix A]:

$$c_d \sin(-\gamma) + \left(1 - \frac{d\gamma}{d\alpha}\right) l_t = 0 \quad (7)$$

where l_t is equal to

$$l_t = \frac{c_d \sin\gamma}{1 + \frac{\frac{d^2 g}{d\alpha^2}}{\sqrt{c_d^2 - \left(\frac{dg}{d\alpha}\right)^2}}} \quad (8)$$

and γ can be written as

$$\gamma = \cos^{-1}\left(\frac{1}{c_d}\frac{dg}{d\alpha}\right). \quad (9)$$

The necessary conditions for the existence of a solution for the VRD synthesis problem are the continuity of $g(\alpha)$ and its derivative. Furthermore, from (8) it has to be noticed that it is necessary that $dg/d\alpha < c_d$. This fact suggests that the idle pulley has to be located at a proper distance from the VRD.

In Appendix B, the VRD synthesis is reported by considering the radius of the idle pulley and the cable thickness.

V. Horizontal Moving Cable Mechanism

Before presenting the prototype of a CBRC, which will be illustrated in Section IV, we propose the schema of a bidimensional HMCM based on a VRD, by applying the theory developed in Section II.

An HMCM (see Fig. 4), which is a module of the crane, is capable of moving a load along a linear path, parallel to the x-axis. This cable-based device can be developed by having recourse just to pulling cables, revolute joints, a regular drum, and a VRD. It has to be noted that no prismatic joints are required.

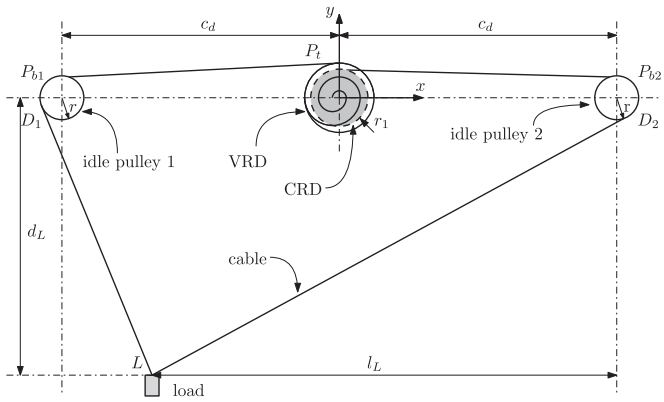

Fig. 4. Graphical representation of a horizontal moving cable mechanism based on a variable radius pulley.

Conventional planar cable-based robots or mechanisms, which act in a vertical plane and are subjected to gravity force, are, in general, two DOFs systems. The most common configuration of this kind of mechanisms is in the form of a triangle, and a load is suspended through two cables between the related motor drums. The two actuators need to be correctly controlled, if, for example, the load has to be carried through a linear path and a trajectory parallel to the ground has to be followed. Hence, the path planning of such systems acts on a two DOFs system. Here, on the contrary, we present a mechanism able to reach the same target using just one DOF.

The HMCM, proposed in Fig. 4, is composed of a VRD, a constant radius pulley (whose radius is r_1 and it is represented in grey), two idle pulleys (that revolute around points $\boldsymbol{P}_{b1}$ and $\boldsymbol{P}_{b2}$ and have each one radius equal to r), and the load. The latter, represented by a little grey rectangle, is assumed to have mass m at point $\boldsymbol{L}$, where m is the third HMCM load for the first two modules whereas the load of the end-effector for the third HMCM. The mechanism is located in the vertical plane and, therefore, gravity force is acting on the mass, which is connected by two cables at point $\boldsymbol{L}$. In this context, we assume cable thickness to be null. The left cable goes around the idle pulley, constrained in $\boldsymbol{P}_{b1}$, and it is then wound around the variable radius pulley. On the contrary, the right cable goes around the idle pulley, fixed in $\boldsymbol{P}_{b2}$, and then it is wound around the constant radius pulley. It has to be noticed that the VRD and the CRD are connected to the same shaft and, therefore, they have the same angular position α. In Fig. 4, c_d indicates the distance between the centers of the lateral pulleys and the center of the variable and constant radius drums, whereas d_L is the distance between the horizontal linear path of the load and the x-axis. Finally, l_L indicates the horizontal distance between point $\boldsymbol{L}$ of the load and the vertical segment intersecting the center of the right idle pulley $\boldsymbol{P}_{b2}$. The angular position α of the VRD is considered positive in the clockwise direction and it is assumed to be null when the load is on the right.

In order to apply the theory developed in Section II, we consider the horizontal moving mechanism in its initial position ($\alpha = 0$, $l_L = 0$). In this configuration, the point $\boldsymbol{L}$ of the load has coordinates $\{c_d, -d_L\}^T$. When the VRD/CRD rotates in the clockwise direction, a segment of the left cable is wound around the variable radius profile whereas, simultaneously, the right cable is released.

By indicating with $\boldsymbol{D}_1$ and $\boldsymbol{D}_2$ the tangency points on the idle pulleys, the synthesis of the VRD profile can be obtained by the following relationship:

$$g(\alpha) = \boldsymbol{D}_1\widehat{(0)\boldsymbol{D}_1}(\alpha) + (||\boldsymbol{L}(0) - \boldsymbol{D}_1(0)|| - ||\boldsymbol{L}(\alpha) - \boldsymbol{D}_1(\alpha)||) \tag{10}$$

where

$$\begin{aligned} ||\boldsymbol{L}(0) - \boldsymbol{D}_1(0)|| &= \sqrt{||\boldsymbol{L}(0) - \boldsymbol{P}_b||^2 - r^2} \\ &= \sqrt{(2c_d)^2 + d_L^2 - r^2} \end{aligned} \tag{11}$$

and

$$||\boldsymbol{L}(\alpha) - \boldsymbol{D}_1(\alpha)|| = \sqrt{(2c_d - l_l(\alpha))^2 + d_L^2 - r^2}. \tag{12}$$

The function $l_L(\alpha)$ expresses the correlation between the VRD angular position and the horizontal translation of the load $\boldsymbol{L}$. It can be written as follows:

$$\begin{aligned} l_L(\alpha) &= \sqrt{||\boldsymbol{L}(\alpha) - \boldsymbol{P}_b||^2 - d_L^2} \\ &= \sqrt{||\boldsymbol{L}(\alpha) - \boldsymbol{D}_2(\alpha)||^2 + r^2 - d_L^2} \end{aligned} \tag{13}$$

where $||\boldsymbol{L}(\alpha) - \boldsymbol{D}_2(\alpha)||$ can be expressed as

$$\begin{aligned} ||\boldsymbol{L}(\alpha) - \boldsymbol{D}_2(\alpha)|| &= ||\boldsymbol{L}(0) - \boldsymbol{D}_2(0)|| + r_1\alpha + \boldsymbol{D}_2\widehat{(0)\boldsymbol{D}_2}(\alpha) \\ &= \sqrt{d_L^2 - r^2} + r_1\alpha - \boldsymbol{D}_2\widehat{(0)\boldsymbol{D}_2}(\alpha). \end{aligned} \tag{14}$$

For the sake of simplicity, the arcs $\boldsymbol{D}_1\widehat{(0)\boldsymbol{D}_1}(\alpha)$ as well as $\boldsymbol{D}_2\widehat{(0)\boldsymbol{D}_2}(\alpha)$ can be considered equal to zero in the numeric implementation. Finally, the analytical function for the synthesis of the VRD profile can be obtained by backward replacing (14), (13), (12), and (11) into (10).

The 3-D model of the VRD obtained by implementing the analytical profile in SolidWorks is reported in Fig. 9.

VI. Inverse Kinematic and Dynamics

The inverse kinematic analysis and the reduced inertia of the CBRC are here presented. With reference to Fig. 5, the function $l_L(\alpha)$ can be expressed as $l_L(\alpha) = c_d - x$, where x is the position of the end-effector in the Cartesian space. With simple trigonometric considerations and by knowing that $\boldsymbol{LP}_{b2} = \sqrt{{l_L}^2 + {d_L}^2}$, it is possible to find the values of angles

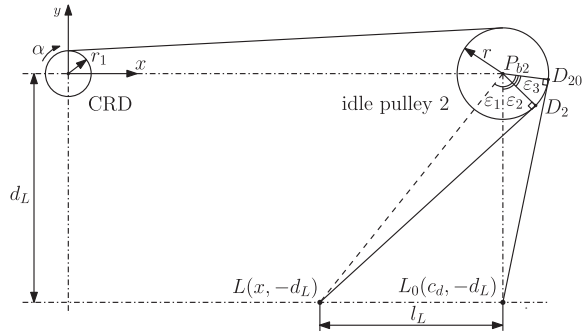

Fig. 5. Inverse kinematic analysis of the HMCM.

ε_1, ε_2, and ε_3 as follows:

$$\begin{aligned} \varepsilon_1 &= a\tan\left(\frac{l_L}{d_L}\right) \\ \varepsilon_2 &= \frac{\pi}{2} - a\sin\left(\frac{r}{\boldsymbol{LP}_{b2}}\right) - \varepsilon_1 \\ \varepsilon_3 &= \frac{\pi}{2} - a\sin\left(\frac{r}{d_L}\right) - \varepsilon_2. \end{aligned} \tag{15}$$

For a given value of the free coordinate α, we can easily calculate the length of an unrolled segment of cable as follows:

$$\begin{aligned} \alpha\, r_1 &= ||\boldsymbol{L}(\alpha) - \boldsymbol{D}_2(\alpha)|| + \boldsymbol{D}_2\widehat{(\alpha)\boldsymbol{D}_2}(0) - ||\boldsymbol{L}(0) - \boldsymbol{D}_2(0)|| \\ &= \sqrt{{l_L}^2 + {d_L}^2 - r^2} + \varepsilon_3\, r - \sqrt{{d_L}^2 - r^2}. \end{aligned} \tag{16}$$

The equation of inverse kinematic $\alpha = \tilde{f}(x)$ is straightforward:

$$\alpha = \frac{1}{r}\left(\sqrt{{l_L}^2 + {d_L}^2 - r^2} - \sqrt{{d_L}^2 - r^2} + \varepsilon_3\, r\right). \tag{17}$$

As far as dynamics is conceived, the reduced inertia I related to the shaft of the VRD can be calculated as follows:

$$I = I_{\text{VRD}} + I_P\, {\tau_{\alpha,\theta_2}}^2 + I_P\, {\tau_{\alpha,\theta_1}}^2 + m\, {\tau_{\alpha,x}}^2 \tag{18}$$

where I_{VRD} is the inertia of the VRD, I_P the inertia of the idle pulley, and m the mass of the load. Furthermore, we indicate with τ_{α,θ_2}, τ_{α,θ_1}, and $\tau_{\alpha,x}$ the transmission ratios between the VRD shaft (which rotates of an angle α) and the right pulley (θ_2), left one (θ_1), and the end-effector (x), respectively. In particular, the contributions of the different transmission ratios can be written as follows:

$$\begin{aligned} \tau_{\alpha,\theta_2} &= \frac{\dot{\theta}_2}{\dot{\alpha}} = \frac{r_1}{r} \\ \tau_{\alpha,x} &= \frac{\dot{x}}{\dot{\alpha}} = \frac{\mathrm{d}\,\tilde{f}^{-1}(\alpha)}{\mathrm{d}\,\alpha} \\ \tau_{\alpha,\theta_1} &= \frac{\dot{\theta}_1}{\dot{\alpha}}. \end{aligned} \tag{19}$$

By considering that

$$\theta_2 = \frac{r_1}{r}\,\alpha = \frac{r_1}{r}\,\tilde{f}(x) \tag{20}$$

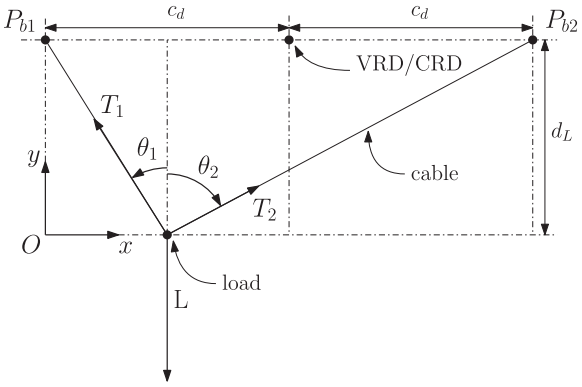

Fig. 6. Graphical representation of cable tensions in the HMCM.

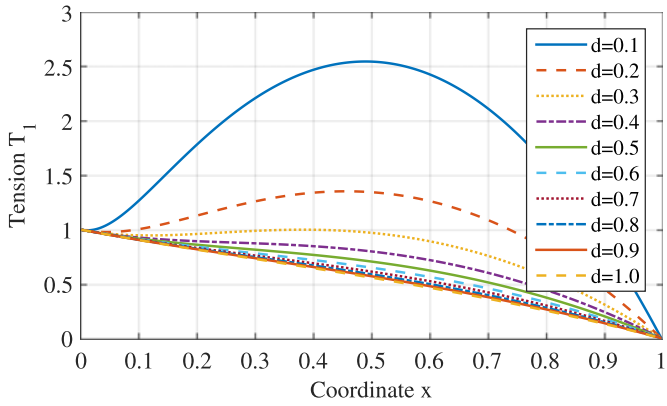

Fig. 7. Tension $\boldsymbol{T}_1$ over the x-axis, for different values of parameter d.

for symmetry, we can easily obtain the expression of θ_1 in function of angle α:

$$\theta_1 = -\frac{r_1}{r}\,\tilde{f}(-x) = -\frac{r_1}{r}\,\tilde{f}(-\tilde{f}^{-1}(\alpha)) \tag{21}$$

where the direct kinematic equation $x = \tilde{f}^{-1}(\alpha)$ has been taken into account.

Finally, by calculating the derivative function with respect to α, the expression of the transmission ratio between the VRD and the idle pulley 1 is obtained:

$$\tau_{\alpha,\theta_1} = \frac{\dot{\theta}_1}{\dot{\alpha}} = \frac{r_1}{r}\frac{\tilde{f}'(-x)}{\tilde{f}'(x)} = \frac{r_1}{r}\frac{\tilde{f}'(-\tilde{f}^{-1}(\alpha))}{\tilde{f}'(\tilde{f}^{-1}(\alpha))}. \tag{22}$$

VII. Cable Tension Analysis

In this section, we present an analysis of tensions in the cables of the CBRC. For the sake of simplicity, we consider the bidimensional horizontal moving mechanism presented in Section III. In Fig. 6, a graphical representation of cable tensions $\boldsymbol{T}_1$ and $\boldsymbol{T}_2$ in the robotic crane is shown. $\boldsymbol{L}$ is the weight force, whereas θ_1 and θ_2 are the angles between the cables and the vertical plane. It has to be noticed that, in this analysis, the idle pulleys as well as the VRD and the CRD are considered to be point-like.

By solving the horizontal and vertical equilibrium equations system, the two tensions can be easily obtained:

$$\boldsymbol{T}_2 = \frac{\boldsymbol{L}}{\sin(\theta_2)\frac{\cos(\theta_1)}{\sin(\theta_1)} + \cos(\theta_2)}$$

$$\boldsymbol{T}_1 = \boldsymbol{T}_2\frac{\sin(\theta_2)}{\sin(\theta_1)}. \tag{23}$$

In order to make the examination nondependent from distance d_L and from interaxle spacing c_d, we introduce the parameter d, defined as $d := d_L/2\,c_d$. Furthermore, the tensions $\boldsymbol{T}_1$ and $\boldsymbol{T}_2$ are divided by the weight force mg, whereas the x-coordinate by the distance $2\,c_d$.

In Fig. 7, the trend of tension $\boldsymbol{T}_1$ over the x-axis, for different values of the parameter d, is reported. It has to be noticed that only tension $\boldsymbol{T}_1$ has been reported, since the two tensions

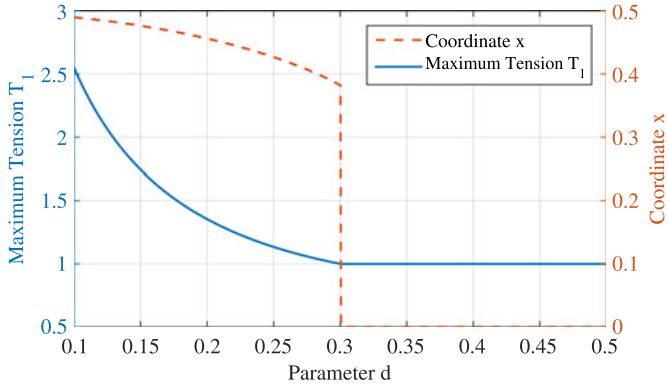

Fig. 8. Maximum tension $\boldsymbol{T}_1$ and its position on the x-axis with respect to d.

are symmetric with respect to the central vertical axis of the mechanism, corresponding to a value of $x = 0.5$.

In Fig. 8, the maximum tension $\boldsymbol{T}_1$ and its position on the x-axis with respect to parameter d are reported. As it can be seen, for $d = 0.3$, a discontinuity point in the position of the x-coordinate is present and, for values of d greater than this value, the maximum tension in the cable is equal to the weight force. This examination can be useful in the first stage of the design of a CBRC, when the vertical distance of the end-effector with respect to the pulleys horizontal height has to be chosen. Additionally, it has to be noticed that the torque required to maintain the load in an equilibrium point is null. This is because the potential energy is constant since the load moves along a horizontal path.

VIII. Prototype of the Cable-Based Robotic Crane

A general overview of the experimental prototype is reported in Fig. 9. Before describing the features of the experimental prototype, it is necessary to underline that the fabrication of a VRD is a critical aspect, since its shape cannot be easily obtained by means of traditional manufacturing processes. In order to obtain a working prototype, we have used 3-D printing fused deposition modeling technology, which allows the creation of free-form shapes by means of a 3-D modeling software. Not only the VRDs, but also the CRDs, the idle pulleys,

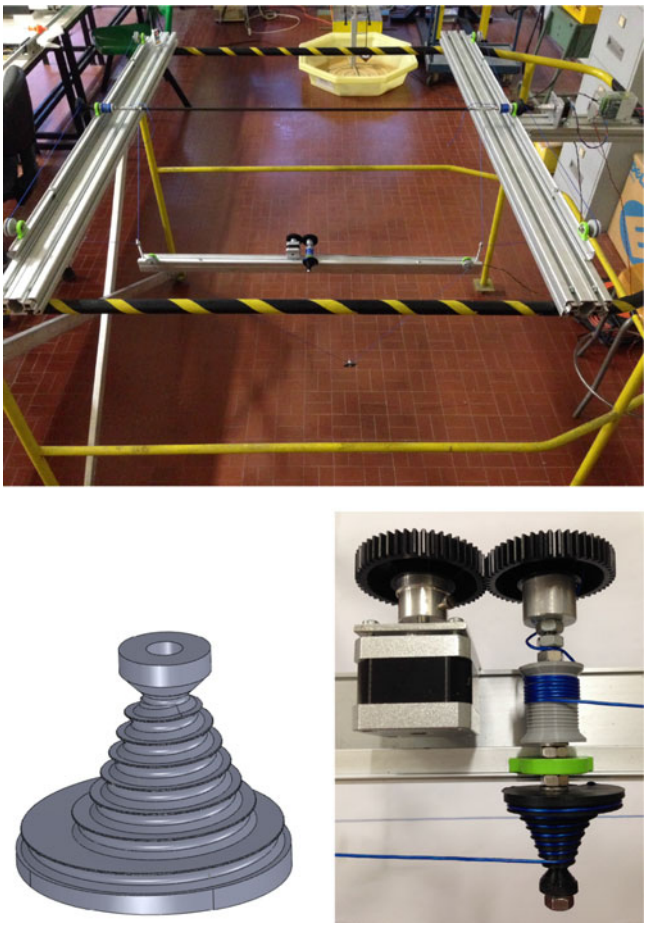

Fig. 9. Experimental prototype of the cable-based robotic crane. On the top, a general overview of the experimental set-up can be seen. On the bottom-right corner, the actuator system, the gear wheels, and VRD 3 are shown, whereas on the bottom-left corner, the 3-D model of the VRD is reported.

and the bearing supports have been produced with 3-D printing technology in PLA plastic. The upper and lower frames of the CBRC have been realized with aluminum profile shapes, whereas the transmission shaft has been built in carbon. With reference to Fig. 4, the geometrical parameters for each of the three single HMCM that composes the experimental CBRC are $c_d = 500\,\text{mm}$, $d_L = 500\,\text{mm}$, $r = 15\,\text{mm}$, and $r_1 = 10\,\text{mm}$. In this prototype, a load with a mass equal to $m = 0.550\,\text{kg}$ has been chosen. As actuators, we used two 12 V powered NEMA 17 stepper motors, which have been chosen for the compact shape, lightweight, and output torque properties. The motors are driven by two L293D drivers directly controlled by an ArduinoUNO rev.3 microcontroller board, based on the ATmega 328P.

In order to measure the cable tensions, we developed a proper measurement system, reported in Fig. 11. It consists of three 3-D printed idle pulleys and a Phidgets microload cell that allow to measure the cable tension in the vertical direction. The load cell has been calibrated and the data acquired by means of a SparkFun OpenScale board.

As it can be noticed from the figures and the graphic representations, the VRDs and the constant radius drums are not planar, but they are in the form of a helical cone and a cylinder, respectively. Except when the spiral angle is less than 360º, purely planar VRDs and CRDs are impossible to build. This fact introduces an error with respect to the mathematical theory developed in Sections III and IV, which is inherent to purely planar mechanisms. As it can be seen in Fig. 9, the idle pulleys and the drums are not coplanar. In fact, as the bearings supports (printed in green plastic) for both idle pulleys and drums shafts are mounted on the same plane, a small offset between the tangent point of the cable on the drums and the tangent point of the cable on the pulleys is present. This deviation produces an error source with respect to the nominal behavior of the mechanism but, for the sake of simplicity, it has been neglected in this context.

Finally, the most important error sources that affect the CBRC can be summarized in the following list.

1) manufacturing errors;
2) mathematical approximation in the VRD synthesis [see (14), namely, $\boldsymbol{D}_1\widehat{(0)\boldsymbol{D}_1}(\alpha) \simeq 0$ as well as $\boldsymbol{D}_2\widehat{(0)\boldsymbol{D}_2}(\alpha) \simeq 0$];
3) nonplanarity of the idle pulleys and drums;
4) geometrical errors;
5) misalignment of the pulleys and drums axis;
6) cables elongation and elasticity [4], [12], [43].
   Cables elongation Δx with respect to the nominal length x_0 can be calculated with the following equation:
   $$\Delta x = \frac{T(x)}{AE}\, x_0 \tag{24}$$
   where $T(x)$ is the cable tension, A is the cross-sectional area of the cable, whereas E is Young's modulus. In the plastic cable employed in our prototype, $EA \simeq 13\,kN$. In particular, with respect to Fig. 6, the accuracy errors Λ_x and Λ_y in the x- and y-directions, due the cable elasticity and relative to the payload, can be evaluated as follows:
   $$\Lambda_x = \frac{|x_E - x_L|}{mg} \quad \Lambda_y = \frac{|y_E - y_L|}{mg} \tag{25}$$
   where (x_L, y_L) and (x_E, y_E) are the end-effector coordinates in nominal position and the ones affected by cable elongations, calculated with (23) and (24). Fig. 10 reports the trend of these errors along the x-axis.
7) scale errors.
   The scale error e_x for a single HMCM (see Fig. 6) affects the measure on the end-effector position along the x-axis, resulting in the following error:
   $$e_x = \frac{(K_1^2 - 1)l_1^2(\alpha) - (K_2^2 - 1)l_2^2(\alpha)}{2L^2} \tag{26}$$
   where K_1 and K_2 are the scale factors on idle pulleys 1 and 2, respectively, $l_1(\alpha)$ and $l_2(\alpha)$ are the length of the free-cables 1 and 2 in function of the free-coordinate α, and $L = 2\,c_d$.

IX. Experimental Results

The performance of the CBRC here presented can be evaluated by measuring the deviation of the end-effector from a

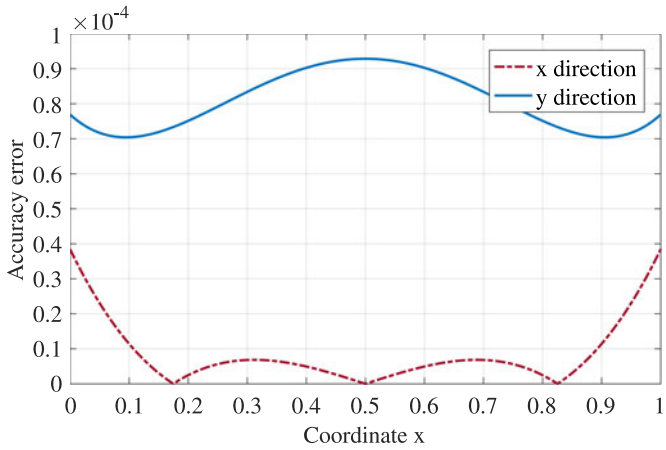

Fig. 10. Accuracy errors Λ_x and Λ_y, relative to the payload, over the x-axis (a value of $d = 0.5$ has been chosen).

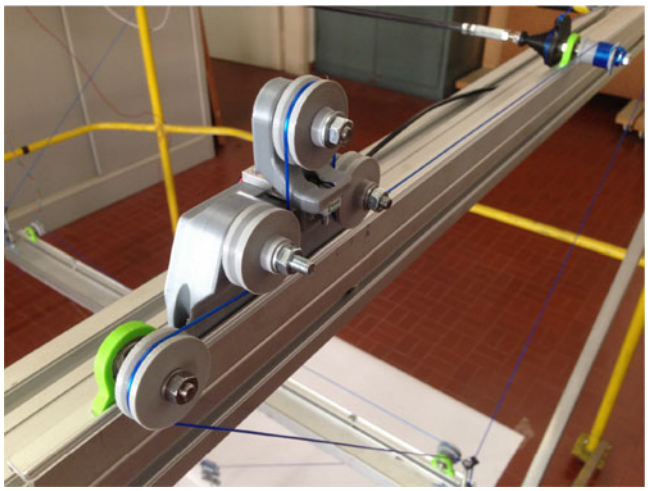

Fig. 11. Cable tension measurement system.

nominal planar surface. In order to do so, a grid has been marked out on the working area of the overhead traveling crane and the height of the load has been measured, under static conditions, by means of a vertical calliper through the surface in both the x- and y-directions. On the working area, a sampling interval has been chosen of $\Delta x = 50\,\text{mm}$ and $\Delta y = 50\,\text{mm}$ starting from ($x = 0$, $y = 0$) till ($x = 700\,\text{mm}$, $y = 700\,\text{mm}$).

In Fig. 12, the experimental results are shown. The red dots indicate the measure points, whereas the blue planar surface is the nominal plane. As it can be seen, the maximum deviation from the theoretic path is actually really small and equal to 5.8 mm. At this value, it corresponds a maximum relative error of 0.83% to the total length of the path in one direction (700 mm). It can be appreciable how the relative error is very small and lower than 1% throughout the whole working area. These results show that the experimental prototype, even in this early stages of development, can achieve its task with acceptable accuracy and precision. Moreover, the offset of the drums does not produce a worrying effect on the performance of the global mechanism. The deviation error could be further reduced by

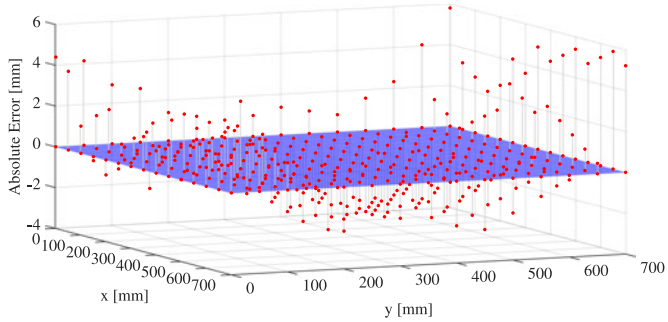

Fig. 12. Absolute experimental error with reference to nominal planar surface.

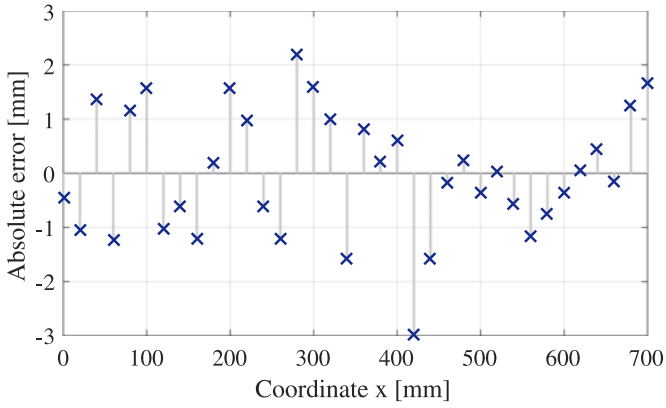

Fig. 13. Absolute experimental error in the x-axis.

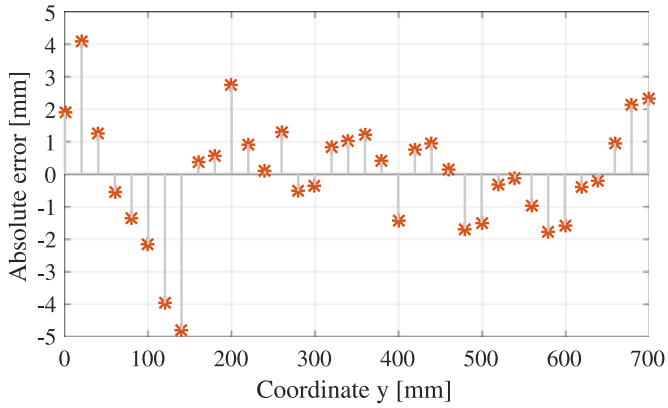

Fig. 14. Absolute experimental error in the y-axis.

using more accurate manufacturing technologies for the VRD and the pulleys, with respect to 3-D printing technique, e.g., milling machine manufacturing.

Furthermore, the errors along the x- and y-axis have been evaluated in order to provide the positional accuracy of the upper and lower HMCMs separately. In particular, errors in the x-direction have been evaluated by fixing the upper HMCMs and moving only the lower HMCM. In the same manner, y errors refer to the center of the frame of the lower HMCM, when only the two upper mechanisms are activated. As we have done for the evaluation of vertical accuracy, measures in the x- and

TABLE I
STATISTICAL ANALYSIS OF ABSOLUTE ERRORS [%]

Axis	Max	Mean	St. Dev.	p-value (K.–S. test)
x	0.4254	0.1352	0.0938	<0.05
y	0.6880	0.1895	0.1626	<0.05
z	0.8326	1.6858	1.1992	<0.05

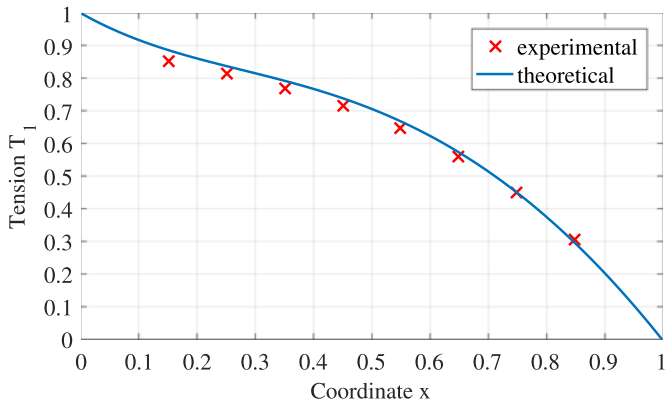

Fig. 15. Tension T_1 over the x-axis, comparison between theoretical and experimental data ($d = 0.5$).

TABLE II
EXPERIMENTAL CABLE TENSION ERRORS IN FUNCTION OF x POSITION WITH RESPECT TO THEORETICAL DATA ($d = 0.5$)

x-coord. [mm]	Max	Mean	St. Dev.
150	0.0556	0.0336	0.0181
250	0.0427	0.0237	0.0173
350	0.0402	0.0237	0.0172
450	0.0421	0.0231	0.0183
550	0.0415	0.0189	0.0191
650	0.0334	0.0159	0.0131
750	0.0224	0.0130	0.0058
850	0.0268	0.0130	0.0095

y-directions have been acquired under static conditions. In fact, measurements have been taken after the dynamic oscillations became negligible. In Figs. 13 and 14, the absolute experimental errors in the x- and y-directions, respectively, are reported. Table I summarizes the statistical analysis of the absolute errors in the three directions. As it can be seen, a Kolmogorov–Smirnov test has been applied to the errors in order to verify the normal distribution of data.

Finally, the cable tensions of the presented prototype have been measured in order to compare them with those previously computed in Section VII (case $d = 0.5$ in Fig. 7). The results are reported in Fig. 15. For each point, six different measures have been acquired and the statistical analysis of the data is reported in Table II. In particular, the results have been divided by mg, where m is the mass of the load used in the measures, in order to compare them with the theoretical data. As it can be seen from Fig. 15, a good agreement between the theoretical curve and the experimental results can be appreciated.

X. CONCLUSION

In this paper, a new family of overhead traveling cranes, based on variable drums and named CBRC, was presented. The direct kinematic analysis and the synthesis of the geometry of a VRD were proposed. The VRD theory was applied first on a bidimensional horizontal moving mechanism and then to a 3-D overhead crane. An experimental prototype of a CBRC, produced using 3-D printing technology, was presented and an analysis of tensions in cables was provided. Finally, the performance of this mechanism was evaluated, and a deviation of the end-effector from the nominal position of less than 1%, throughout the whole working area in the x-, y-, and z-directions, was found. Furthermore, the cable tensions have been measured and compared with the theoretical values.

The presented prototype of the CBRC highlights the advantages of using VRDs with respect to traditional CDRs, the first and foremost being the simplicity in the required actuation system. In fact, it is well known that one would need several CRDs with a coupled actuation system to drive them in a synchronous manner in order to make the end-effector moving along a linear path on a planar surface. On the other hand, the VRD requires only to compensate the variation of the radius, in order to produce a demanded speed or torque output. Moreover, the CBRC here described is characterized by a lighter weight with respect to traditional overhead traveling cranes, it is reconfigurable and modular. It has to be noticed that in this preliminary prototype, oscillation and vibration effects might occur during the end-effector motion. Even if this problem raises also in traditional overhead traveling cranes, in the presented experimental system, the cables flexibility as well as the pendulum phenomena might introduce negative issues during the movement of the load. From a practical perspective, where stiffness might be required by several applications, this aspect needs to be further investigated, e.g., by implementing antiswing as well as vibration-suppression control strategies [23]. Furthermore, the maximum speed of the system depends on the size of the cables and their tensions, as well as its acceleration is limited by the cables stability, since they support traction but no compression. Such problems have been addressed in other cable robots, where gravity forces are involved [44].

This research study has reached remarkable results in the application of VRDs to cable-based overhead cranes. Nevertheless, improvements can be done in the manufacturing of the complex shapes of VRDs profiles. Furthermore, a complete sensitivity analysis of CBRC kinematics would be useful to evaluate potential issues before providing interesting real applications. In the future, we plan to further investigate cable-driven cranes based on VRDs. In particular, the safety of the system in the case of cable failure [45] can be analyzed and the elongation of the cables [12] can be taken into account.

APPENDIX A
MATHEMATICAL DERIVATIONS OF THE VRD SYNTHESIS

In this appendix, the mathematical derivations of the VRD profile synthesis are reported.

For the further calculations, it is to be noticed that

$$\frac{d\boldsymbol{T}(x)}{dx} = \boldsymbol{T}\left(x+\frac{\pi}{2}\right). \tag{27}$$

In particular, by differentiating (6) with respect to angle α, we can obtain

$$\begin{aligned}\frac{d\boldsymbol{P}_t}{d\alpha} &= \frac{d\boldsymbol{T}(\alpha)}{d\alpha}\left\{\begin{array}{c} c_d \\ 0 \end{array}\right\} + \frac{d\boldsymbol{T}(\alpha)}{d\alpha}\boldsymbol{T}(-\gamma)\boldsymbol{T}\left(-\frac{\pi}{2}\right)\left\{\begin{array}{c} l_t \\ 0 \end{array}\right\} \\ &\quad -\frac{d\gamma}{d\alpha}(\alpha)\frac{d\boldsymbol{T}(-\gamma)}{d(-\gamma)}\boldsymbol{T}(\alpha)\boldsymbol{T}\left(-\frac{\pi}{2}\right)\left\{\begin{array}{c} l_t \\ 0 \end{array}\right\} \\ &= \boldsymbol{T}\left(\alpha+\frac{\pi}{2}\right)\left\{\begin{array}{c} c_d \\ 0 \end{array}\right\} + \boldsymbol{T}(\alpha)\boldsymbol{T}(-\gamma)\left(1-\frac{d\gamma}{d\alpha}\right)\left\{\begin{array}{c} l_t \\ 0 \end{array}\right\}. \end{aligned} \tag{28}$$

The unit vector normal to the VRD profile in tangent point $\boldsymbol{P}_t$ is

$$\boldsymbol{n} = \boldsymbol{T}(\alpha)\boldsymbol{T}(\boldsymbol{-\gamma})\left\{\begin{array}{c} 1 \\ 0 \end{array}\right\}. \tag{29}$$

Since $d\boldsymbol{P}_t/d\alpha$ points at any time along the tangent line $\boldsymbol{P}_t\boldsymbol{P}_b$, it is normal to unit vector $\boldsymbol{n}$. This orthogonality relationship can be written as

$$\boldsymbol{n}^T\frac{d\boldsymbol{P}_t}{d\alpha} = 0. \tag{30}$$

By substituting (28) and (29) into (30) and by using the property of orthogonal matrices $\boldsymbol{T}^T\boldsymbol{T} = \boldsymbol{I}$, it follows

$$\left\{\begin{array}{cc} 1 & 0 \end{array}\right\}\boldsymbol{T}^T(-\gamma)\boldsymbol{T}\left(\frac{pi}{2}\right)\left\{\begin{array}{c} c_d \\ 0 \end{array}\right\} + \left(1-\frac{d\gamma}{d\alpha}\right)\left\{\begin{array}{cc} 1 & 0 \end{array}\right\}\left\{\begin{array}{c} l_t \\ 0 \end{array}\right\} = 0$$

$$c_d\sin(-\gamma) + \left(1-\frac{d\gamma}{d\alpha}\right)l_t = 0. \tag{31}$$

The relationship between the lever arm l_a, the unrolled cable length, and the VRD rotation angle α is $l_a = dg/d\alpha$. In particular, from Fig. 3, it can be easily seen that $c_d\cos(\gamma) = l_a$. By combining the two previous equations, we obtain $c_d\cos(\gamma) = dg/d\alpha$. At this stage, we can differentiate the previous relationship and, by considering that $c_d\sin(\gamma) = \sqrt{c_d^2 + l_a^2}$, we obtain

$$\frac{d\gamma}{d\alpha} = -\frac{\frac{d^2g}{d\alpha^2}}{\sqrt{c_d^2 - \left(\frac{dg}{d\alpha}\right)^2}}. \tag{32}$$

Appendix B
VRD Synthesis by Considering the Radius of the Idle Pulley and the Cable Thickness

In the following, we introduce the radius r of the idle pulley and the thickness of the cable $2f$. The radius r includes the radius of the idle pulley and half of the cable thickness. In Fig. 16, a graphical representation of this configuration is reported. Similarly to what is stated in (6), the geometry of the VRD can be now expressed as

$$\boldsymbol{P}_t = \boldsymbol{T}(\alpha)\left\{\begin{array}{c} c_d \\ 0 \end{array}\right\} + \boldsymbol{T}(\alpha)\boldsymbol{T}(-\gamma)\boldsymbol{T}\left(-\frac{\pi}{2}\right)\left\{\begin{array}{c} l_t \\ 0 \end{array}\right\} + \chi(\alpha) \tag{33}$$

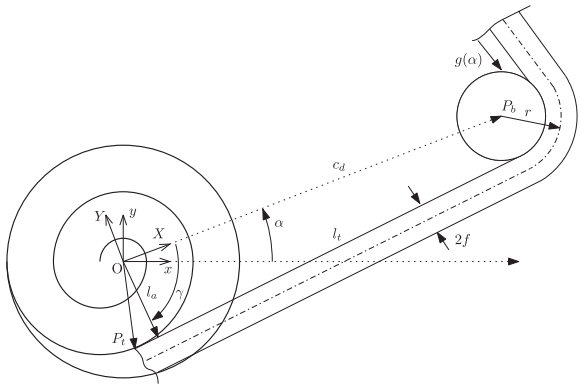

Fig. 16. Variable radius drum parameters by considering the radius of the idle pulley and the cable thickness.

where the function $\chi(\alpha)$ is equal to

$$\chi(\alpha) = \boldsymbol{T}(\alpha-\gamma)\left\{\begin{array}{c} r \\ 0 \end{array}\right\} - \boldsymbol{T}(\gamma+\alpha)\left\{\begin{array}{c} f \\ 0 \end{array}\right\}. \tag{34}$$

We can express the vector tangent to the profile in $\boldsymbol{P}_t$ as

$$\begin{aligned}\frac{d\boldsymbol{P}_t}{d\alpha} &= \frac{d\boldsymbol{T}(\alpha)}{d\alpha}\left\{\begin{array}{c} c_d \\ 0 \end{array}\right\} + \frac{d\boldsymbol{T}(\alpha)}{d\alpha}\boldsymbol{T}(-\gamma)\boldsymbol{T}\left(-\frac{\pi}{2}\right)\left\{\begin{array}{c} l_t \\ 0 \end{array}\right\} \\ &\quad -\frac{d\gamma}{d\alpha}(\alpha)\frac{d\boldsymbol{T}(-\gamma)}{d(-\gamma)}\boldsymbol{T}(\alpha)\boldsymbol{T}\left(-\frac{\pi}{2}\right)\left\{\begin{array}{c} l_t \\ 0 \end{array}\right\} + \frac{d\chi(\alpha)}{d\alpha} \\ &= \boldsymbol{T}\left(\alpha+\frac{\pi}{2}\right)\left\{\begin{array}{c} c_d \\ 0 \end{array}\right\} + \boldsymbol{T}(\alpha)\boldsymbol{T}(-\gamma)\left(1-\frac{d\gamma}{d\alpha}\right)\left\{\begin{array}{c} l_t \\ 0 \end{array}\right\} \\ &\quad + \frac{d\chi(\alpha)}{d\alpha} \end{aligned} \tag{35}$$

since

$$\begin{aligned}\frac{d\chi(\alpha)}{d\alpha} &= \frac{d\boldsymbol{T}(\alpha-\gamma)}{d\alpha}\left(1-\frac{d\gamma}{d\alpha}\right)\left\{\begin{array}{c} r \\ 0 \end{array}\right\} \\ &\quad - \frac{d\boldsymbol{T}(\alpha-\gamma)}{d\alpha}\left(1-\frac{d\gamma}{d\alpha}\right)\left\{\begin{array}{c} f \\ 0 \end{array}\right\} \\ &= \boldsymbol{T}\left(\alpha-\gamma+\frac{\pi}{2}\right)\left(1-\frac{d\gamma}{d\alpha}\right)\left\{\begin{array}{c} r \\ 0 \end{array}\right\} \\ &\quad + \boldsymbol{T}\left(\alpha-\gamma+\frac{\pi}{2}\right)\left(1-\frac{d\gamma}{d\alpha}\right)\left\{\begin{array}{c} f \\ 0 \end{array}\right\}. \end{aligned} \tag{36}$$

It has to be noticed that (35) is equal to (28). Consequently, the orthogonality condition of (30) leads to the same results of (8) and (9). In fact

$$\boldsymbol{n}^T\frac{d\chi(\alpha)}{d\alpha} = 0. \tag{37}$$

Finally, we obtain that the geometry of the VRD profile, in Cartesian coordinates, is given by (33), associated with (8), (9), and (34).

Acknowledgment

The authors would like to thank Mr. F. Bacciocchini for his help in setting up the system.

REFERENCES

[1] S. Seriani, P. Gallina, and A. Wedler, "A modular cable robot for inspection and light manipulation on celestial bodies," *Acta Astron.*, vol. 123, pp. 145–153, 2016.

[2] J. Albus, R. Bostelman, and N. Dagalakis, "The NIST robocrane," *J. Robot. Syst.*, vol. 10, no. 5, pp. 709–724, 1992.

[3] P. Bosscher, R. L. Williams, L. S. Bryson, and D. Castro-Lacouture, "Cable-suspended robotic contour crafting system," *Autom. Construction*, vol. 17, no. 1, pp. 45–55, 2007.

[4] Z. N. Masoud, "Effect of hoisting cable elasticity on anti-sway controllers of quay-side container cranes," *Nonlinear Dyn.*, vol. 58, no. 1, pp. 129–140, 2009.

[5] S. Lahouar, E. Ottaviano, S. Zeghoul, L. Romdhane, and M. Ceccarelli, "Collision free path-planning for cable-driven parallel robots," *Robot. Auton. Syst.*, vol. 57, no. 11, pp. 1083–1093, 2009.

[6] R. L. Williams, J. S. Albus, and R. V. Bostelman, "Self-contained automated construction deposition system," *Autom. Construction*, vol. 13, no. 3, pp. 393–407, 2004.

[7] J.-B. Izard, M. Gouttefarde, C. Baradat, D. Culla, and D. Sallé, "Integration of a parallel cable-driven robot on an existing building façade," in *Cable-Driven Parallel Robots*. New York, NY, USA: Springer, 2013, pp. 149–164.

[8] J.-P. Merlet and D. Daney, "A portable, modular parallel wire crane for rescue operations," in *Proc. 2010 IEEE Int. Conf. Robot. Autom.*, 2010, pp. 2834–2839.

[9] G. Rosati, P. Gallina, S. Masiero, and A. Rossi, "Design of a new 5 DOF wire-based robot for rehabilitation," in *Proc. 9th Int. Conf. Rehabil. Robot.*, 2005, pp. 430–433.

[10] D. Zanotto, G. Rosati, S. Minto, and A. Rossi, "Sophia-3: A semiadaptive cable-driven rehabilitation device with a tilting working plane," *IEEE Trans. Robot.*, vol. 30, no. 4, pp. 974–979, Aug. 2014.

[11] B. Kehoe *et al.*, "Autonomous multilateral debridement with the raven surgical robot," in *Proc. 2014 IEEE Int. Conf. Robot. Autom.*, 2014, pp. 1432–1439.

[12] L. S. Chiang, P. S. Jay, P. Valdastri, A. Menciassi, and P. Dario, "Tendon sheath analysis for estimation of distal end force and elongation," in *Proc. IEEE/ASME Int. Conf. Adv. Intell. Mechatron.*, 2009, pp. 332–337.

[13] J. Mahler *et al.*, "Learning accurate kinematic control of cable-driven surgical robots using data cleaning and Gaussian process regression," in *Proc. 2014 IEEE Int. Conf Autom. Sci. Eng.*, 2014, pp. 532–539.

[14] T. Do, T. Tjahjowidodo, M. Lau, and S. Phee, "Real-time enhancement of tracking performances for cable-conduit mechanisms-driven flexible robots," *Robot. Comput.-Integr. Manuf.*, vol. 37, pp. 197–207, 2016.

[15] L. L. Cone, "Skycam-An aerial robotic camera system," *Byte*, vol. 10, no. 10, pp. 122–132, 1985.

[16] M. Filipović, "The importance of modelling an aerial robotic camera," *Sci. Tech. Rev.*, vol. 62, no. 1, pp. 28–37, 2012.

[17] M. Hiller, S. Fang, S. Mielczarek, R. Verhoeven, and D. Franitza, "Design, analysis and realization of tendon-based parallel manipulators," *Mech. Mach. Theory*, vol. 40, no. 4, pp. 429–445, 2005.

[18] J. Pusey, A. Fattah, S. Agrawal, and E. Messina, "Design and workspace analysis of a 6–6 cable-suspended parallel robot," *Mech. Mach. Theory*, vol. 39, no. 7, pp. 761–778, 2004.

[19] S.-R. Oh, K. K. Mankala, S. K. Agrawal, and J. S. Albus, "Dynamic modeling and robust controller design of a two-stage parallel cable robot," *Multibody Syst. Dyn.*, vol. 13, no. 4, pp. 385–399, 2005.

[20] S.-R. Oh and S. K. Agrawal, "Cable suspended planar robots with redundant cables: Controllers with positive tensions," *IEEE Trans. Robot.*, vol. 21, no. 3, pp. 457–465, Jun. 2005.

[21] S. Oh and S. K. Agrawal, "A reference governor-based controller for a cable robot under input constraints," *IEEE Trans. Control Syst. Technol.*, vol. 13, no. 4, pp. 639–645, Jul. 2005.

[22] P. Gallina and A. Trevisani, "Synthesis and experimental validation of a delayed reference controller for active vibration suppression in mechanical systems," *J. Appl. Mech.*, vol. 72, no. 4, pp. 623–627, 2005.

[23] P. Gallina and A. Trevisani, "Delayed reference control of a two-mass elastic system," *Modal Anal.*, vol. 10, no. 1, pp. 135–159, 2004.

[24] J. Gorman, K. W. Jablokow, and D. J. Cannon, "The cable array robot: Theory and experiment," in *Proc. IEEE Int. Conf. Robot. Autom.*, vol. 3, 2001, pp. 2804–2810.

[25] Y. Lu and D. Fan, "Transmission backlash of precise cable drive system," *Proc. Inst. Mech. Eng. C, J. Mech. Eng. Sci.*, vol. 227, no. 10, pp. 2256–2267, 2013.

[26] S.-W. Ji, S.-J. Kim, and Y.-B. Kim, "Experimental approach for mooring winch control system design," in *Proc. 2013 13th Int. Conf. Control, Autom. Syst.*, 2013, pp. 1025–1028.

[27] J. M. Lincoln, D. L. Lucas, R. W. McKibbin, C. C. Woodward, and J. E. Bevan, "Reducing commercial fishing deck hazards with engineering solutions for winch design," *J. Safety Res.*, vol. 39, no. 2, pp. 231–235, 2008.

[28] E. Kilic, M. Dolen, and A. B. Koku, "Experimental evaluation of cable-drum systems as linear motion sensors," in *Proc. 2011 IEEE Int. Conf. Mechatron.*, 2011, pp. 666–671.

[29] E. Kilic and M. Dolen, "Prediction of slip in cable-drum systems using structured neural networks," in *Proc. Inst. Mech. Eng. C, J. Mech. Eng. Sci.*, vol. 228, no. 3, pp. 441–456, 2014.

[30] D. Shin, X. Yeh, and O. Khatib, "Circular pulley versus variable radius pulley: Optimal design methodologies and dynamic characteristics analysis," *IEEE Trans. Robot.*, vol. 29, no. 3, pp. 766–774, Jun. 2013.

[31] S. Seriani and P. Gallina, "Variable radius drum mechanisms," *J. Mech. Robot.*, vol. 8, no. 2, 2016, Art. no. 021016.

[32] G. Endo, H. Yamada, A. Yajima, M. Ogata, and S. Hirose, "A passive weight compensation mechanism with a non-circular pulley and a spring," in *Proc. 2010 IEEE Int. Conf. Robot. Autom.*, 2010, pp. 3843–3848.

[33] M. Kilic, Y. Yazicioglu, and D. F. Kurtulus, "Synthesis of a torsional spring mechanism with mechanically adjustable stiffness using wrapping cams," *Mech. Mach. Theory*, vol. 57, pp. 27–39, 2012.

[34] N. Schmit and M. Okada, "Synthesis of a non-circular cable spool to realize a nonlinear rotational spring," in *Proc. 2011 IEEE/RSJ Int. Conf. Intell. Robots Syst.*, 2011, pp. 762–767.

[35] B. Kim and A. D. Deshpande, "Design of nonlinear rotational stiffness using a noncircular pulley-spring mechanism," *J. Mech. Robot.*, vol. 6, no. 4, 2014, Art. no. 041009.

[36] D. Shin, X. Yeh, and O. Khatib, "Variable radius pulley design methodology for pneumatic artificial muscle-based antagonistic actuation systems," in *Proc. 2011 IEEE/RSJ Int. Conf. Intell. Robots Syst.*, 2011, pp. 1830–1835.

[37] E. Kljuno, J. J. Zhu, R. L. Williams, and S. M. Reilly, "A biomimetic elastic cable driven quadruped robot: The robocat," in *Proc. ASME 2011 Int. Mech. Eng. Congr. Expo*, 2011, pp. 759–769.

[38] P. Gallina, "A new class of rocker-belt mechanisms," *Mech. Mach. Theory*, vol. 40, no. 8, pp. 963–976, 2005.

[39] H.-H. Lee, "Modeling and control of a three-dimensional overhead crane," *J. Dyn. Syst., Meas. Control*, vol. 120, no. 4, pp. 471–476, 1998.

[40] Y. Fang, W. Dixon, D. Dawson, and E. Zergeroglu, "Nonlinear coupling control laws for an underactuated overhead crane system," *IEEE/ASME Trans. Mechatron.*, vol. 8, no. 3, pp. 418–423, Sep. 2003.

[41] J. Yi, N. Yubazaki, and K. Hirota, "Anti-swing and positioning control of overhead traveling crane," *Inf. Sci.*, vol. 155, no. 1, pp. 19–42, 2003.

[42] S.-G. Lee *et al.*, "Partial feedback linearization control of a three-dimensional overhead crane," *Int. J. Control, Autom. Syst.*, vol. 11, no. 4, pp. 718–727, 2013.

[43] Y. B. Bedoustani, H. D. Taghirad, and M. M. Aref, "Dynamics analysis of a redundant parallel manipulator driven by elastic cables," in *Proc. 10th Int. Conf. Control, Autom., Robot. Vision*, 2008, pp. 536–542.

[44] L. Pigani and P. Gallina, "Cable-direct-driven-robot (CDRR) with a 3-link passive serial support," *Robot. Comput.-Integr. Manuf.*, vol. 30, no. 3, pp. 265–276, 2014.

[45] G. Boschetti, C. Passarini, and A. Trevisani, "A strategy for moving cable driven robots safely in case of cable failure," in *Advances in Italian Mechanism Science*. New York, NY, USA: Springer, 2017, pp. 203–211.

Lorenzo Scalera received the Bachelor's degree in industrial engineering and the Master's degree in mechanical engineering, both with honors, from the University of Trieste, Trieste, Italy, in 2012 and 2015, respectively. He is currently working toward the Ph.D. degree in applied mechanics and robotics at the University of Udine, Udine, Italy.

His research interests include the fields of cable robots, haptics, human–robot interaction, collaborative robotics for artistic applications, and dynamic modeling of flexible-link mechanisms.

Paolo Gallina received the Master's degree in mechanical engineering from the University of Padova, Padova, Italy, in 1996 and the Ph.D. degree in applied mechanics from the University of Brescia, Brescia, Italy, in 1999.

He is currently an Associate Professor of applied mechanics with the Department of Civil Engineering and Architecture, University of Trieste, Trieste, Italy. He was a Visiting Professor with the Ohio University, Athens, OH, in 2000/1. In 2002, he implemented a hands-on Mechatronic Laboratory for students in Engineering. In 2003, he implemented a Robotics Laboratory, where he carries out his main research in robotics. In 2004, he was a Visiting Professor with Colorado University, Boulder, CO, USA, at the Centre for Advanced Manufacturing and Packaging of Microwave, Optical and Digital Electronics, in order to collaborate on mechatronics and micromechanics fields. He was the Head of the Council for Students in Mechanical Engineering degree from 2004 to 2008, and the Head of the Master's program: "Safety and hygiene in the working environment" from 2006 to 2008. His research interests include vibrations, human–machine interfaces, robotics, especially applied to rehabilitation.

Stefano Seriani was born in Trieste, Italy, in 1986. He received the B.E. degree in industrial engineering in 2010, the M.Sc. degree in mechanical engineering in 2012, and the Ph.D. degree in applied mechanics and robotics from the University of Trieste, Trieste, Italy, 2016.

In 2016, he was a Research Fellow with the Institute of Robotics and Mechatronics of the German Space Agency (DLR). He is currently a Research Fellow with the University of Trieste. His research interests include space robotics, applied mechanics, computer vision, and image processing.

Alessandro Gasparetto received the Master's degree in electronic engineering from the University of Padova, Padova, Italy in 1992; the Master's degree in mathematics from the University of Padova, Padova, Italy in 2003; and the Ph.D. degree in mechanics applied to machines from the University of Brescia, Brescia, Italy in 1996.

He is currently a Full Professor of mechanics of machines with the Polytechnic Department of Engineering and Architecture, University of Udine, Udine, Italy, where he is the Head of the research group in Mechatronics and Robotics and has several scientific and institutional appointments. He is currently a Vice-Rector for quality assurance with the University of Udine, and the President of the International Federation for the Promotion of Mechanism and Machine Science (IFToMM) Italy, a Member Organization of IFToMM. He is the author of about 180 international publications and of three patents in the field of industrial automation. His research interests include the fields of modeling and control of mechatronic systems, robotics, mechanical design, industrial automation, and mechanical vibrations.